THE PUBLISHING HOUSE
OF THE ROMANIAN ACADEMY

PROCEEDINGS OF THE ROMANIAN ACADEMY, Series A,
Volume 18, Number 3/2017, pp.248–255

FLOW FIELD EVOLUTION IN STENTED *VERSUS* STENOSED CORONARY ARTERY

Alin F. TOTOREAN[1], Claudia I. HUDREA[2], Alin I. BOSIOC[1], Sandor I. BERNAD[3]

[1] "Politehnica" University of Timisoara, Department of Mechanical Machines, Equipment and Transportation, Timisoara, Romania
[2] "Victor Babes" University of Medicine and Pharmacy Timisoara, Timisoara, Romania
[3] Romanian Academy, Centre of Fundamental and Advanced Research in Engineering Sciences, Timisoara Branch, Timisoara
Corresponding author: Sandor I. Bernad, e-mail: sandor.bernad@upt.ro

Abstract. Stent deployment alters the geometric flow boundary conditions, due to the protrusion of stent struts into the flow stream. The flow field in the vicinity of the stent wires demonstrated the presence of the stagnation zones. The pressure falls rapidly both of the investigated geometries. Downstream to the stenosis throat and the stented segment respectively, there is a tendency for pressure recovery due to flow deceleration. The vascular deformations modify the flow velocity profiles and facilitate the development of the recirculation zone, defined by low values corresponding to the wall shear stress.

Key words: stent, re-stenosis, stenosis, wall shear stress, pressure drop.

1. INTRODUCTION

For the treatment of coronary atherosclerotic lesions, stenting is the most commonly performed procedure during the percutaneous interventions.

Many strategies have been attempted to eliminate the acute artery response like neointimal hyperplasia (NH) and in-stent restenosis (ISR), developed after stent insertion [1]. Initialization of the NH is the result of the altered hemodynamics in stented artery. A presence of the stent causes abnormal shear stresses on the endothelial cells resulting an excessive growth of tissue in and around the implanted stent, resulting in a decreased blood flow through the vessel [2].

Stent deployment alters the geometric flow boundary conditions, due to the protrusion of stent struts into the flow stream, resulting alteration of the local blood flow patterns. Detailed and accurate quantification of the local hemodynamics requires computational methods. Computational fluid dynamics (CFD) can provide detailed information on critical flow parameters including information near the stent struts and the arterial wall respectively. Different CFD studies have been proposed in the literature, where researchers investigated an idealized model [3–5], or image-based stented artery models [6, 7].

The objective of the present paper is to quantify the flow field both in stenosed artery geometry and geometry obtained after stent implantation, taking into the geometric particularity of the investigated regions.

2. NUMERICAL SETUP

In the present study, the hemodynamic characteristics of the blood flow through the stented coronary artery model are investigated. Our results provide data regarding the hemodynamic parameters for the blood flow in the coronary stent under physiological conditions, namely wall shear stress and pressure drop.

Stent geometry. Although the coronary circulation is extremely complex, but in present study a very simple model was chosen for initial studies contained a straight rigid tube with stenotic elements and respectively a rigid tube with simple stent struts geometry used for stented artery investigations.

The stent geometry used for flow analysis (particularly for the wall shear stress – WSS analysis around the strut, and across the bed of the host tube) are presented in Figs. 1 and 2. For numerical and experimental investigations, we used a simplified geometry model where the internal diameter of the coronary artery was taken to be $D = 8$ mm and the stent inner diameter was $D_i = 7.92$ mm. The investigated geometry model was larger than the real artery (diameter of 4 mm), showing a ration of 2:1. Geometrical characteristics of both stenosed and stented artery are presented in Table 1.

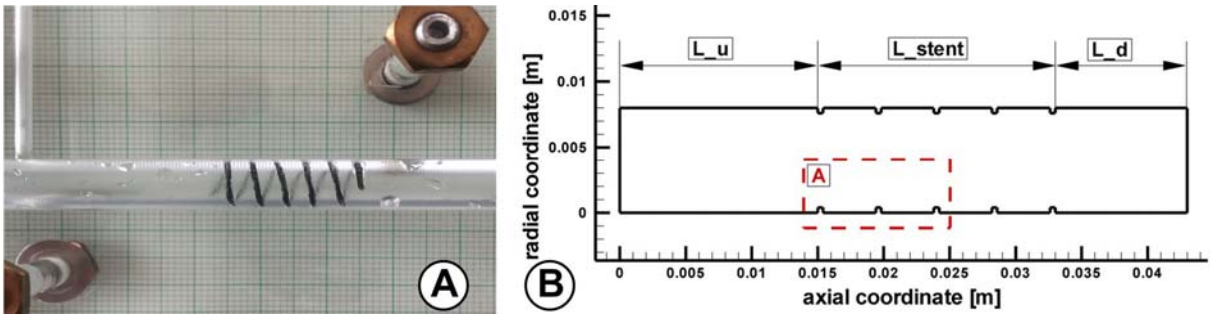

Fig. 1 – The experimental and computational domain used for stent hydrodynamics investigations.

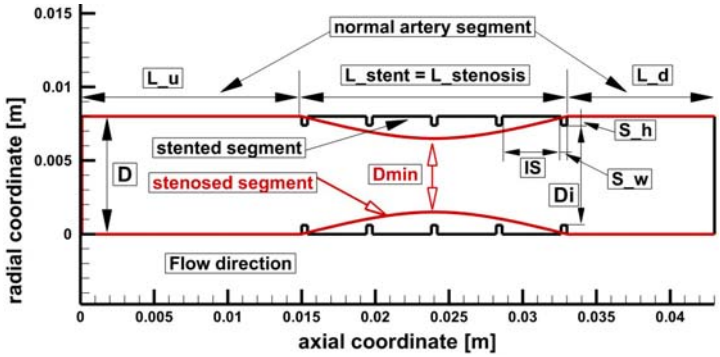

Fig. 2 – Stenosed artery and stented artery, computational domain.

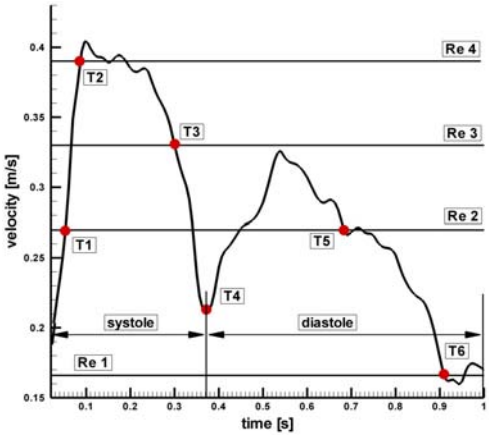

Fig. 3 – Time steps along the imposed cardiac cycle used in numerical simulations.

Table 1

Investigated geometry details

Nr.	*L*_u [mm]	*L*_d [mm]	*L*_st [mm]	*D*i [mm]	*L*_stenosis [mm]	*D* [mm]	*D*min [mm]	Geometry length [mm]
1	15	10	18	7.92	18	8	5	43

Table 2

Stent geometry descriptions

Nr.	*S*_h [mm]	*S*_w [mm]	IS [mm]	No. of row
1	0.4 = H	0.4	3.8	5

Boundary Conditions. The present analysis was performed for a different moment at the velocity waveform obtained from a patient with severe coronary pathology where stent implantation would perform (Fig. 2). To simplify the analysis, fluid was assumed to be a homogeneous, incompressible and Newtonian. The simulations were done under steady flow condition corresponding to the different time steps along the imposed cardiac cycle (Fig. 3). The assumptions for the numerical simulation are the following: flow laminar, gravitational effects are negligible, and the physical properties remain constant.

A plug flow velocity profile was imposed at the inlet of the vessel. Inlet section is long enough to allow the fully developed flow in the investigated stented artery section [8]. Consequently at the inlet: a uniform

inflow velocity profile for the axial velocity component and a zero transverse velocity component are used. Here V_{inlet} = 0.35 m/s (based on Reynolds number of 360). Outlet: the outlet pressure was defined to be 0 Pa. Wall: the vessel wall was assumed to be rigid and non-slip, considering that blood vessel prostheses usually deform little under pressure. The fluid is assumed incompressible having a dynamic viscosity (μ) of 0.00408 Pa.s and a density (ρ) of 1050 kg/m3. The bypass walls are considered rigid and impermeable. The numerical simulation is performed using the commercial CFD software FLUENT 6.3 [9].

3. RESULTS AND DISCUSSION

Flow visualization and analysis. We carried out flow visualizations both in the stented coronary artery and in the stenosed artery (Fig. 4) for different Reynolds numbers presented along the investigated cardiac cycle (T2 and T6 shown in Fig. 3). Velocity field and the corresponding recirculation zones around the stented area in the two-dimensional model are shown in Fig. 4a.

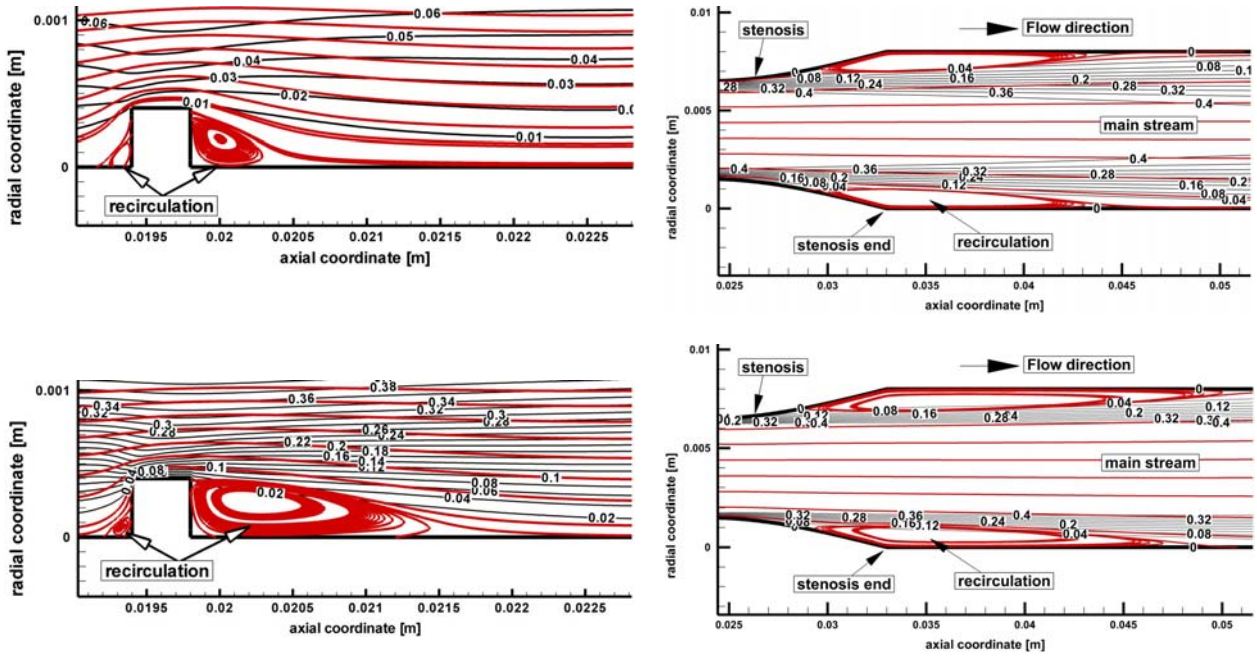

a) b)

Fig. 4 – Velocity magnitude (red line) and flow streamtrace (black line) corresponding to two different time steps, top row time = T6 and bottom row time = T2. a) stented geometry; b) stenosed geomtery – distal segment of the stenosed artery. (For interpretation of the references to color in this figure legend, the reader is referred to the web version of this article.)

Fluid perturbations start to appear at the tip of the strut. A clockwise vortex forms at the beginning of systole and reach the maximum size during the peak systolic time (time T2 – Fig. 4a bottom). Stagnation and recirculation areas are captured in Fig. 4 for both stenosed and stented artery.

The flow field in the vicinity of the stent wires demonstrated the presence of the stagnation zones. This zone size is depended directly by the wire spacing. These stagnation zones contained vortices where the velocities represent a small fraction of the velocities observed above the stent wires (Fig. 4). For all investigated time steps, the stagnation zone upstream of the wires was smaller than the stagnation zone downstream of the wires.

Figure 5 present comparisons between experimentally and numerically obtained flow fields in the stented artery. Similar flow patterns can be found and reported in some recent investigations [10–13]. Flow disturbances through these vessel segments were observed as the colored dye was released at a near wall position of the vessel proximal to the test section. Dye streamlines were recorded by the video camera as they passed through the stented segment of the artery.

Since the secondary flow caused by the presence of the struts is expected to be strongly dependent on the strut geometry characteristics (height and width). This geometric factor will influence the spatial and temporal variations of the velocity field.

The absence of a recirculation region may be advantageous since this reduces the contact between blood and the artificial graft surface and consequently minimize the risk of the thrombosis.

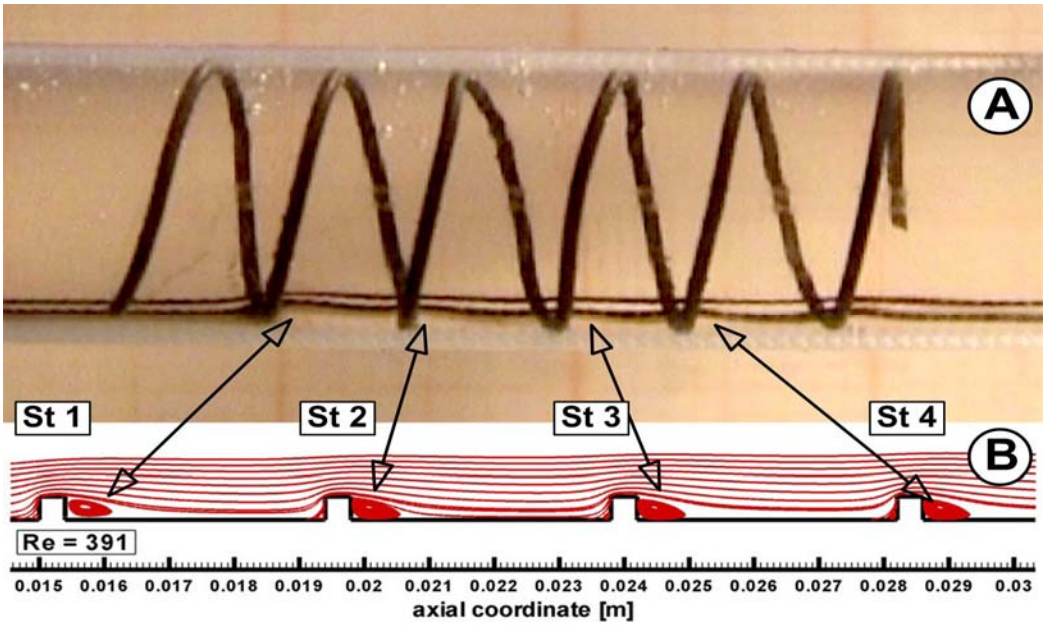

Fig. 5 – a) Experimental flow visualizations in the stented segment (custom-built nonclinical stent used in experimental investigations); b) flow field around stent struts obtained using numerical simulation. Artery diameter of 8 mm, 5 row of struts, stent geometry of 43 mm length. Figure A is not a scale.

These observations become particularly significant when coupled with clinical evidence concerning different rates of ISR attributed at various stent geometries [8]. For example, neointimal growth over the luminal aspect of the stented artery alters the flow boundary geometry and the local flow parameters. Therefore, CFD studies with fixed geometry are strictly only valid for the acute stage of implantation, i.e., in the first week [4, 8].

Pressure distribution

To assess the effect of the stenosis in the distal artery section, pressure drop analysis across the stenosis is a crucial element. It is demonstrated that the pressure drop across a constricted area with a specified geometry is expressible in the following form:

$$\frac{\Delta p}{\rho U^2} = f\left(\frac{Z}{D}, \frac{A_1}{A_0}, \frac{L}{D}, \mathrm{Re}\right), \tag{1}$$

where Δp is the pressure drop over the length Z (stenosis or stent), A_1 and A_0 are the unobstructed and obstructed areas respectively, L is stenosis/stent length, and D unobstructed artery diameter. Thus, the pressure drop is a function of the Reynolds number, area reduction and length of the stenosis or stented segment. As it follows from equation 1, the pressure drop is a result of energy dissipation in the stenosed or stented artery segment.

The pressure falls rapidly in the investigated artery (both for stenosed and stented segment) primarily due to the Bernoulli effect as the flow accelerates. Downstream to the throat, there is a tendency for pressure recovery due to flow deceleration (Fig. 6). For the cases of stented artery pressure recovery was obtained in the vicinity of the last stent strut, but for the case of stenosed segment pressure recovery was downstream to the stenosis throat due to the flow deceleration. In such cases, the total pressure drop becomes primarily a

function of minimum stenosis area and relatively independent of the detailed geometry. For both geometries (stenosed and stented artery) at low Reynolds numbers, viscous effects dominate and no pressure recovery is observed (Fig. 6).

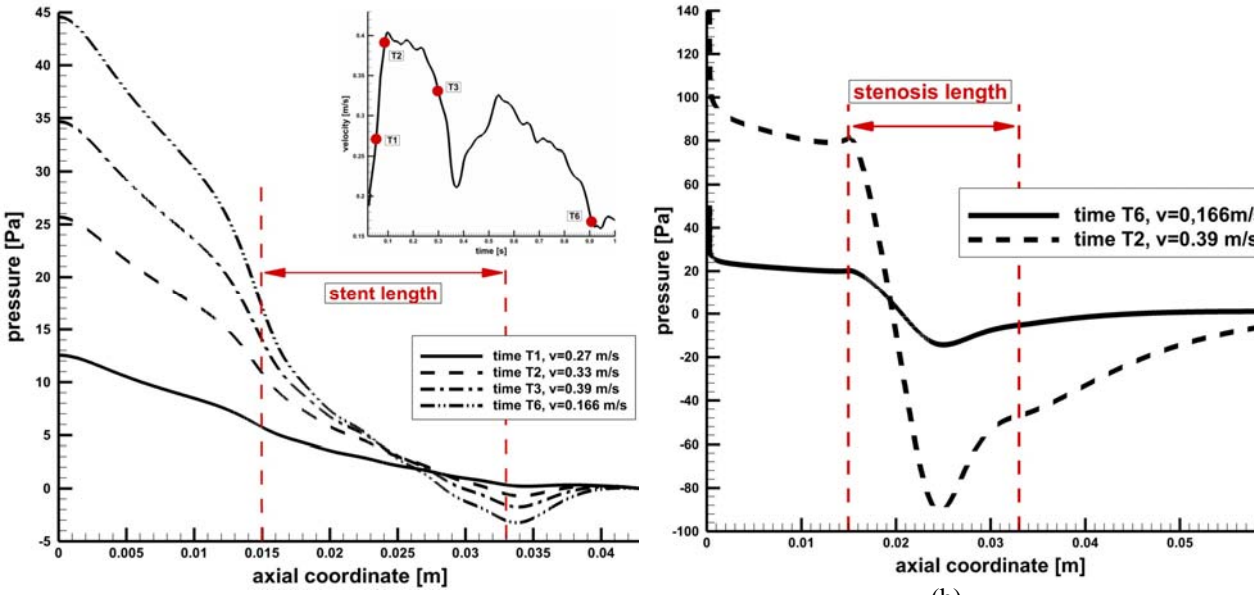

(a) (b)

Fig. 6 – Axial pressure distribution corresponding to different investigated time steps: a) pressure distribution in the stented artery; b) pressure distribution in the stenosed artery.
In both geometries, we can find the pressure recovery tendency after restricted zone.

Wall shear stress distribution. Wall shear stress (WSS) are the tangential stress derived from the friction of flowing blood on the endothelial surface, is determined by flow velocity and by the presence of geometry asymmetries or the obstructions [14]. Implantation of rigid stent frameworks imposes acute alterations to the 3-dimensional arterial geometry and creates focal irregularities related to the strut protrusion [15].

The threshold for comparing distributions of low WSS between simulations was established at 5 dynes/cm^2 for comparison to previous work [16]. Because vascular regions are subjected to WSS, below this value, have been shown a strong correlation with sites of intimal thickening [17].

Stent-induced changes in arterial geometry and, consequently, in flow and WSS patterns modify the arterial response to endothelial injury, thereby increasing the risk of in-stent restenosis (ISR) and stent thrombosis (ST). Low values of WSS have been recognized as critical for neointimal hyperplasia (NH). Endothelial cells subjected toWSS lower than 0.4 Pa or oscillatory WSS are circular in shape without any preferred flow alignment pattern. These cells, coupled with the blood stagnation usually observed in regions of low WSS, lead to increased uptake of blood-borne particles to the arterial wall, which is prevalent in atherosclerosis, as a result of increased residence time and increased permeability of the endothelial layer [4]. These vascular deformations modify the flow velocity profiles, reduce the post-implantation WSS along the entire length of the stent, and alter the focal in-stent WSS distribution [16]. The presence of a recirculation zone induces low values corresponding to the wall shear stress. Increasing the Reynolds number recirculation zone increase and reach the maximum length of 2 mm for the case of Re 4 (Figs. 4a and 7).

A low wall shear stress zone (< 0.28 Pa, for the case of Re1) is seen downstream to each stent strut corresponding to the recirculation region create distal to the strut. The minimum wall shear stress value for investigated Reynolds number ranges between 0.28 Pa and 1.6 Pa (Fig. 7). The mean average wall shear stress between stent struts reaches the value of 2.1 Pa (Fig. 7). Cells in these pronounced areas of low WSS

are more likely to participate in the neointimal response [17]. As it can be seen in Fig. 7 the wall shear stress distribution for the rectangular designs used in our analysis has two peaks at the upstream and downstream corners of the struts, where the flow velocity increases significantly over a small distance.

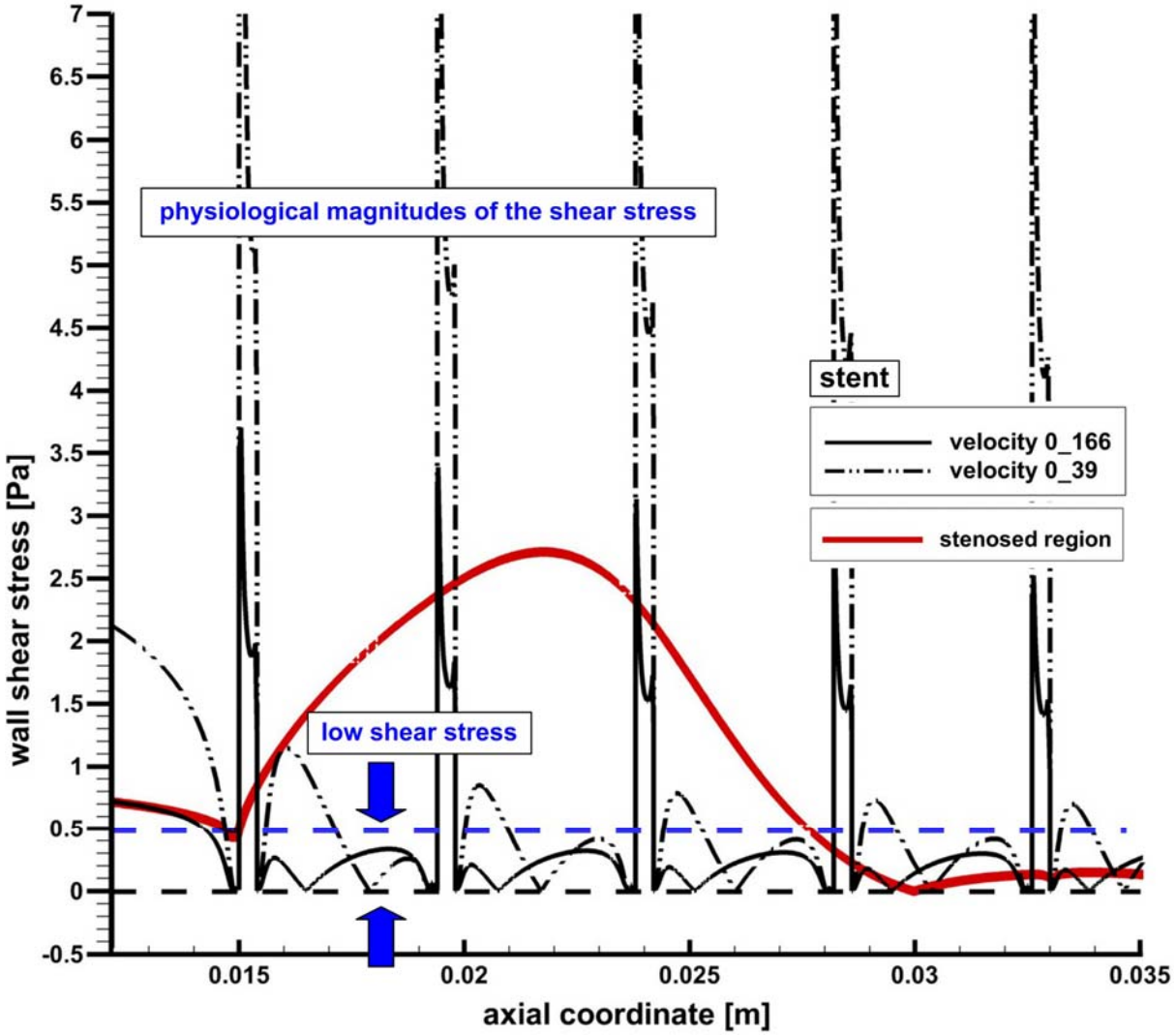

Fig. 7 –Comparison of the wall shear stress distributions between stented and stenosed artery corresponding to different investigated time steps. Wall shear stress threshold value definition used in disease quantification.

Wall shear stress in stenosed and stented artery. To inhibit thrombogenesis the ideal surface consists of an intact endothelium in an atheroprotective flow environment. Due to the stent placement, is a high probability of partial endothelial denudation [18] that initiate a procoagulant surface environment. A high shear rate environment has identified as a condition for endothelialization, but shear stresses in excess of 38 Pa inhibit endothelial cell attachment [19]. Depending on the geometric characteristics of the stent strut cross-section, the local flow environment can promote, retard, or inhibit endothelialization [16, 19].

The areas, where small axial wall shear stress was observed, included: (1) the near wall just beyond of the each strut, (2) the proximal region of the each strut where almost stagnant zone was seen (Figs. 7 and 8). Stenting creates regions with accelerated flow and high WSS on top of the struts and low WSS downstream of the struts. Activated platelets enter in the flow separation zones downstream of struts were reach high concentrations due to delayed flow and the low WSS-mediated attenuation of native anticoagulants may trigger the coagulation cascade.

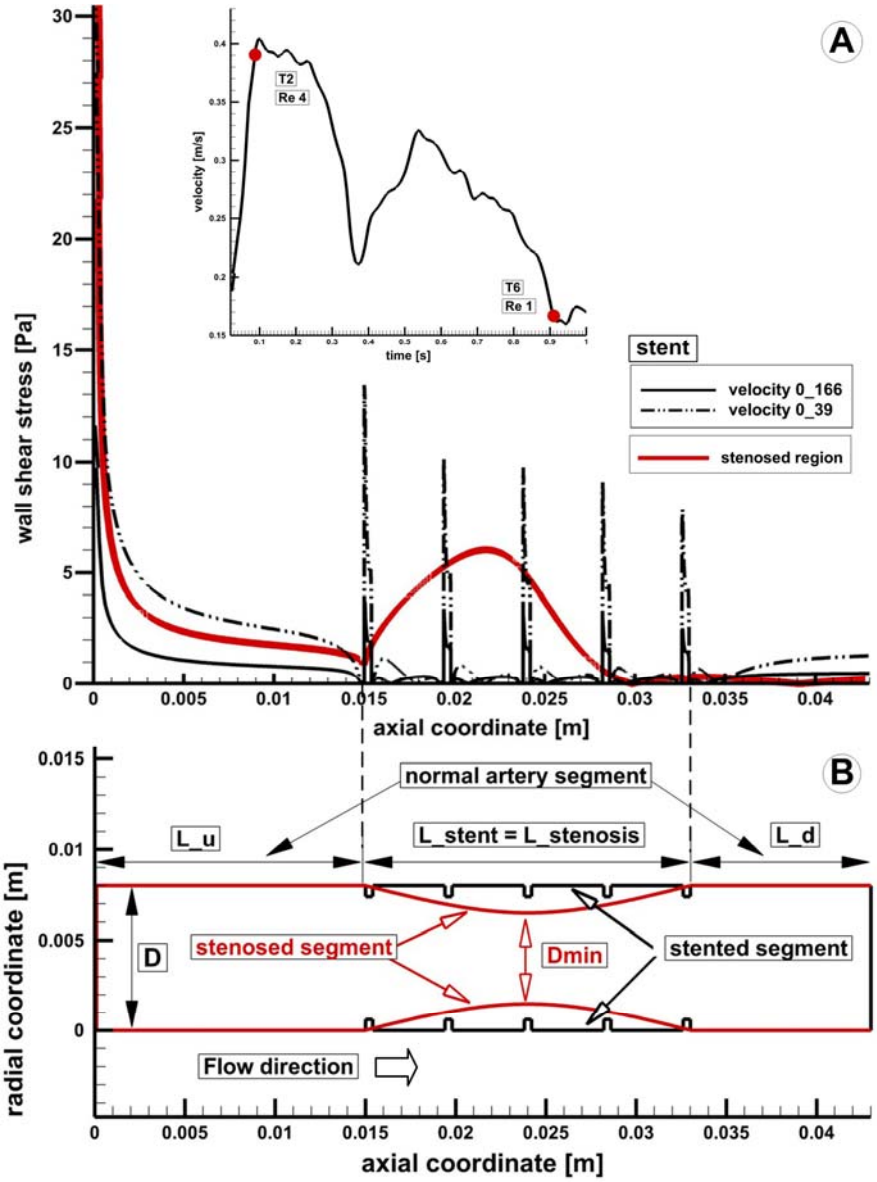

Fig. 8 – Wall shear stress (WSS) evolution in both investigated cases: stenosed and stented artery: a) WSS distribution for two-time steps; b) WSS localization along the investigated geometries.WSS evolution in the vicinity of each stent strut.

4. CONCLUSIONS

In summary, these research studies can guide the development of stent geometry design to provide local flow conditions that minimize platelet adhesion while maximizing endothelial cells growth. The results of 2-D simulation provide the qualitative information on the nature of peak values of the significant parameters in both the time and space domains. They can also provide a solid qualitative understanding of the main centerline flow characteristics, and facilitate the flow parametric studies. Thereby, a more smooth fluid dynamic environment can be supplied, that promotes a more favorable tissue response during the acute stage of stent implantation, to minimize the possibility of the restenosis. As illustrated by these research studies, CFD can provide a critical role in the understanding of such issues.

Thicker and non-streamlined stent designs, such as currently applied rectangular geometries, precipitate stent thrombosis by 1) magnifying high WSS-induced platelet activation on top of struts; and 2) impeding re-endothelialization, in low-WSS regions downstream of struts [14]. Our results presented in Figs. 7 and 8 are correlated well with results obtained by Chatzizisis [14]. Computational predictions

comparing clinically used stents affirm increased platelet deposition in nonstreamlined strut designs that produce complex flow patterns [9, 10].

The current results require interpretation within of several potential limitations. The stent is implanted in idealized computational geometry, and flow simulation in the stenosed artery was performed using a simplified axisymmetric stenosed coronary artery model.

ACKNOWLEDGMENTS

This work has been supported by the CCTFA/LHC 2013–2015 research programme of the Romanian Academy.

REFERENCES

1. PARK S.-J., KANG, S.-J.,VIRMANI R., NAKANO M., UEDA Y., *In-stent neoatherosclerosis: a final common pathway of late stent failure*, J. Am. Coll. Cardiol., **59**, pp. 2051–2057, 2012.
2. WENTZEL J.J., GIJSEN F.J.H., SCHUURBIERS J.C.H., VAN DER STEEN A.F.W., SERRUYS P.W., *The influence of shear stress on in-stent restenosis and thrombosis*, EuroIntervention, **4** (Supl.C), pp. C27–C32, 2008.
3. GUNDERT T.J., DHOLAKIA R.J., MCMAHON D., LADISA JR. J.F., *Computational fluid dynamics evaluation of equivalency in hemodynamic alterations between Driver, Integrity, and similar stents implanted into an idealized coronary artery*, J. Med. Devices, **7**, 011004, 2013.
4. MURPHY J.B., BOYLE F.J., *Predicting neointimal hyperplasia in stented arteries using time-dependant computational fluid dynamics: a review*, Comput. Biol. Med., **40**, pp. 408–418, 2010.
5. PANT S., BRESSLOFF N.W., FORRESTER A.I.J., CURZEN N., *The influence of strut-connectors in stented vessels: a comparison of pulsatile flow through five coronary stents*, Ann. Biomed. Eng., **38**, pp. 1893–1907, 2010.
6. MIGLIAVACCA F, MARTINEZ M.A., MALVE M., CHIASTRA C, *On the necessity of modelling fluid–structure interaction for stented coronary arteries*, Journal of the Mechanical Behavior of Biomedical Materials, **34,** pp. 217–230, 2014
7. ELLWEIN L.M., OTAKE H., GUNDERT T.J., KOO B., SHINKE T., HONDA Y., SHITE J., LaDISA JR. J.F., *Optical coherence tomography for patient-specific 3D artery reconstruction and evaluation of wall shear stress in a left circumflex coronary artery*, Cardiovasc. Eng. Technol, **2**, pp. 212–227, 2011.
8. LaDISA J.F.J., OLSON L.E., GULER I., HETTRICK D.A., AUDI S.H., KERSTEN J.R., WARLTIER D.C., PAGEL P.S., *Stent design properties and deployment ratio influence indexes of wall shear stress: a three-dimensional computational fluid dynamics investigation within a normal artery*, J. Appl. Physiol., **97**, pp. 424–430, 2004.
9. FLUENT 6.3 User's Guide, ANSYS-Fluent Incorporated, (2006).
10. O'BRIEN C.C., KOLACHALAMA V.B., BARBER T.J., SIMMONS A., EDELMAN E.R., *Impact of flow pulsatility on arterial drug distribution in stent-based therapy*, Journal of Controlled Release, **168**, pp. 115–124, 2013.
11. BENARD N., COISNE D., DONAL E., PERRAULT R., *Experimental study of laminar blood flow through an artery treated by a stent implantation: characterisation of intra-stent wall shear stress*, J. Biomech., **36**, pp. 991–998, 2003.
12. TOTOREAN A.F., BOSIOC A.I., BERNAD S.I., SUSAN-RESIGA R., *Identification and visualization of vortices in by-pass graft flow*, Proceedings of the Romanian Academy Series A, **15**, *1*, pp. 52–59, 2014.
13. BERNAD E.S., BERNAD S.I., CRAINA M.L., *Hemodynamic parameters measurements to assess severity of serial lesions in patient specific right coronary artery*, Bio-Medical Materials and Engineering, **24**, *1*, pp. 323–334, 2014.
14. CHATZIZISIS Y.S., COSKUN A.U., JONAS M. *et al*., *Role of endothelial shear stress in the natural history of coronary atherosclerosis and vascular remodeling: molecular, cellular, and vascular behavior*, J. Am. Coll. Cardiol., **49**, pp. 2379 –93, 2007.
15. WENTZEL J.J., WHELAN D.M., VAN DER GIESSEN W.J. *et al*., *Coronary stent implantation changes 3-D vessel geometry and 3-D shear stress distribution*, J. Biomech., **33**, pp. 1287–95, 2003.
16. LaDISA J.F. JR., GULER I., OLSON L.E. *et al*., *Three-dimensional computational fluid dynamic modeling of alterations in coronary wall shear stress produced by stent implantation*, Ann. Biomed. Eng., **31**, pp. 972–80, 2003.
17. DANENBERG H.D., WELT F.G., WALKER M., SEIFERT P., TOEGEL G.S., EDELMAN E.R., *Systemic inflammation induced by lipopolysaccharide increases neointimal formation after balloon and stent injury in rabbits*, Circulation, **105**, pp. 2917–2922, 2002.
18. LIU S.Q., TIECHE C., TANG D., ALKEMA P., *Pattern formation of vascular smooth muscle cells subject to nonuniform fluid shear stress: role of PDGF-beta receptor and Src*, Am. J. Physiol. Heart Circ. Physiol., **285**, pp. H1081–90, 2003.
19. MARTIN K.A., RZUCIDLO E.M., MERENICK B.L. *et al*., *The mTOR/p70 S6K1 pathway regulates vascular smooth muscle cell differentiation*, Am. J. Physiol. Cell. Physiol., **286**, pp. C507–17, 2004.

Received September 14, 2015